CHEMISTRY OF MATERIALS

ARTICLE

pubs.acs.org/cm

Impact of the Growth Conditions of Colloidal PbS Nanocrystals on Photovoltaic Device Performance

Huiying Fu,[†] Sai-Wing Tsang,[†] Yanguang Zhang,[†] Jianying Ouyang,[‡] Jianping Lu,[*,†] Kui Yu,[*,‡] and Ye Tao[*,†]

[†]Institute for Microstructural Sciences, and [‡]Steacie Institute for Molecular Sciences, National Research Council of Canada, Ottawa, Ontario K1A 0R6, Canada

Supporting Information

ABSTRACT: Here, we present a detailed investigation on the influence of the growth conditions of colloidal lead sulfide (PbS) nanocrystals on photovoltaic device performance. The PbS nanocrystals were synthesized in a noncoordinating solvent, 1-octadecene, using oleic acid (OA) as the ligand. It was found that both the feeding molar ratio of OA to Pb and the reactant concentration were critical for controlling the growth rate of nanocrystals. Transient photocurrent (TPC) measurements revealed reduced trap density in thin films using the slow-growth nanocrystals. Solar cells based on the slow-growth nanocrystals showed a high power conversion efficiency (PCE) of 3.8% under simulated Air Mass 1.5 Global (AM 1.5G) irradiation (100 mW/cm^2), a 2-fold increase in PCE, compared to the fast-growth nanocrystals, because of the remarkable improvement in the open-circuit voltage and fill factor in the PV devices.

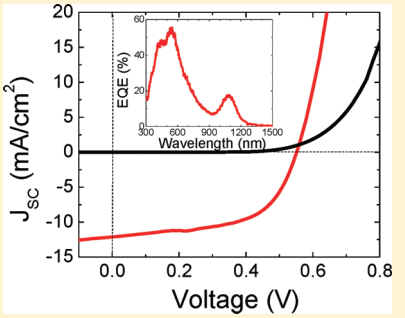

KEYWORDS: PbS nanocrystals, photovoltaic devices, nanocrystal growth rate, transient photocurrent measurement

INTRODUCTION

Colloidal semiconductor nanocrystals (NCs) have attracted tremendous attention, because of their distinct, size-dependent optical, electronic, and mechanical properties,[1,2] as well as their promising technological applications in optoelectronics,[3,4] chemical sensing,[5] biological imaging,[6,7] and etc. It has been recognized that fully passivated surfaces, well-controlled size, and narrow particle size distribution are among the critical parameters for achieving high-quality nanocrystals. Undoubtedly, the quality of the NCs has a direct impact on the electronic and optical properties and the performance of the resulting devices.[8−10]

Because of the broad-band absorption and strong quantum confinement,[11,12] lead chalcogenide nanocrystals have been extensively explored for applications in photovoltaic (PV) devices,[13−17] photodetectors,[18] telecommunications,[19] light-emitting diodes (LED),[20] and thermoelectric devices.[21] Among this group of materials, PbS nanocrystals have demonstrated very promising results in photodetector and PV applications. It is well-known that the growth kinetics of nanocrystals plays a key role in determining the quality of the NC. Scholes and co-workers first reported the synthesis of size-tunable PbS nanocrystals (first exciton peak ranged from 800 nm to 1800 nm), using lead oxide (PbO) and bis(trimethylsilyl) sulfide [$(TMS)_2S$] as the lead and sulfur precursors, respectively.[22] The as-synthesized nanocrystals were isolated from the reaction solution, redispersed in organic solvent, and then underwent a size-focusing aging process to obtain almost-monodispersed PbS nanocrystals (size distribution of 10%−15%). Several attempts have been reported to modify the recipe to enhance the passivation of the nanocrystals, such as diluting oleic acid (OA) in 1-octadecene (ODE), and introducing trioctylphosphine (TOP) as a co-ligand.[10,16,23] Photovoltaic devices based on these PbS nanocrystals only reached a power conversion efficiency (PCE) of 1.6%−1.8%.[13,16,24] More recently, Sargent et al. reported high-performance PbS nanocrystal-based solar cells (3.6%) by replacing the oleic acid with a shorter and tightly bound dithiocarbamate derivative as the surface ligand.[25] Moreover, several reports on heterojunction NC PV cells show further improvement on both device efficiency and stability.[26−30] Nozik et al. has demonstrated long-term stable PV devices that employ PbS/ZnO heterojunctions.[28] Over 5% PCE has also recently been obtained in a PbS/TiO_2 heterojunction device by Sargent et al.[29]

It has been demonstrated by Yu and Peng[31] that an optimized reaction system for growing high-quality nanocrystals can be achieved by manipulating the monomer reactivity with appropriate ligand concentration in a noncoordinating solvent. However, no systematic study has been reported on the correlation between the growth rate of nanocrystals and the performance of the resulting electronic devices. In this work, we adopted and further modified the approach of Yu and Peng to control the growth kinetics of PbS nanocrystals using PbO and $(TMS)_2S$ as the lead and sulfur precursors, respectively. We have found that the growth rate is highly dependent on the OA:Pb molar ratio and the reactant concentration. By tuning the above two parameters, we can prolong the size-focused period of nanocrystal growth from a few seconds to more than one hour. The slow-growth nanocrystals showed reduced trap density, narrow size-distribution, well self-assembled pattern, and long-term storage stability. The nanocrystals synthesized with different growth rates were used to fabricate PV devices. It was found that the

Received: November 2, 2010
Revised: February 25, 2011
Published: March 10, 2011

devices fabricated using slow-growth nanocrystals gained 2-fold increase in PCE, with remarkable open-circuit voltage (V_{OC}) and fill factor (*FF*).

EXPERIMENTAL SECTION

Materials. Lead(II) oxide (PbO) (99.999%), 1-octadecene (ODE) (tech. grade, 90%), oleic acid (tech. grade, 90%), bis(trimethylsilyl) sulfide [$(TMS)_2S$] (synthesis grade), tetrachloroethylene (TCE) (reagent grade, 99+%), anhydrous 2-propanol (99.5%), anhydrous hexanes (99+%), anhydrous chloroform (99+%), anhydrous acetonitrile (99.8%) and 1,3-benzenedithiol are all purchased from Sigma−Aldrich Co. and used as received.

Synthesis of PbS Nanocrystals. In this typical recipe, the molar ratio of OA to Pb was 12:1 and the OA concentration was 0.51 mol/kg. PbO (446.6 mg, 2.0 mmol), OA (6.775 g, 24 mmol), and ODE (50.0 mL) were loaded in a 100-mL three-necked flask. The mixture was degassed and heated up to 100 °C and vacuumed for 1 h to form lead oleate and dry the solution. The solution was cooled down to 90 °C and $(TMS)_2S$ (210 μL, 1.0 mmol) in ODE (5 mL) was swiftly injected into the flask with vigorous stirring under dry nitrogen. The reaction mixture was kept at 85 °C for 3.0 min and quenched by pouring the mixture into anhydrous 2-propanol (150 mL) under N_2 protection. The products were centrifuged and the mixture of PbS nanocrystals and unreacted lead oleate were collected. The nanocrystals were then redissolved in 5 mL anhydrous hexanes, and the undissolved lead oleate was removed by centrifuging at 4000 rpm for 3 min. The nanocrystals were reprecipitated by adding 5 mL acetone (dried over molecular sieves) into the obtained supernatant. The PbS nanocrystals were collected by flocculating the materials with a mixture of acetone and hexanes (1:1) and centrifuging twice. The nanocrystals were dried under a stream of nitrogen and then dissolved in TCE for photophysical characterization.

Photophysical Characterization. A Cary 5000 UV−vis−NIR spectrophotometer and a Photon Technology International (PTI) fluorescence system were used for UV−vis absorption and photoluminescence measurements, respectively. The reaction progress was monitored by timed removal of the aliquot samples from the reaction flask using standard Schlenk technique. Extreme care was taken to avoid the introduction of air and moisture. A Philips CM20 scanning transmission electron microscope (STEM) was used to collect bright-field (BF) TEM images, and a JEOL JEM-2100F field-emission-source TEM was used for high-resolution TEM (HR-TEM) imaging. Samples of PbS nanocrystals in hexanes were drop-cast on carbon-coated TEM copper grids for imaging. Cross-linked PbS nanocrystals for TEM imaging were prepared by adding one drop of 0.02 M 1,3-benzenedithiol solution in acetonitrile on top of the PbS nanocrystals deposited on the copper grids. X-ray diffraction (XRD) data were acquired at room temperature with a Bruker Axs D8 X-ray diffractometer using Cu Kα radiation in a $\theta-\theta$ mode, and the data were collected between 5° and 80° in 2θ with a step size of 0.1° and a counting time of 5 s per step. Samples for XRD were prepared by depositing the purified nanocrystals on low-background quartz plates. X-ray photoelectron spectroscopy (XPS) was performed using a Kratos Axis Ultra XPS equipped with a monochromated Al source. The binding energy was calibrated to the adventitious C 1s at 285 eV. Samples for XPS were prepared by spin-casting a layer of purified PbS nanocrystals (~40 nm thick) on a silicon wafer substrate. FTIR spectra were recorded on a Midac M1200-SP3 spectrophotometer. The FTIR sample was prepared by spin-coating PbS NCs (15 nm in thickness) on a silicon substrate. For transient photocurrent (TPC) measurement, the same structure as the Schottky-type PbS nanocrystal PV device was prepared as described below. The sample was housed inside a cryostat with a base pressure of 10^{-6} Torr at room temperature. The sample was connected in series with a voltage source and a sensing resistor to form a closed circuit. The resulting RC constant was ~10 μs. In order to generate a photocurrent, the PbS nanocrystal thin film was excited by a pulsed nitrogen laser (337 nm and 5 ns) from the ITO side of the device. The temporal photocurrent was finally collected at zero voltage bias with an oscilloscope through the sensing resistor.

Photovoltaic Device Fabrication and Characterization. Schottky-type PbS nanocrystal PV devices were fabricated on ITO coated glass substrate. Immediately prior to device fabrication, the ITO glass was cleaned by ultrasonic baths of organic solvents (acetone and isopropanol) and UV-ozone treatment for 15 min. A 5 mg/mL solution of PbS-OA in chloroform was used to prepare the active layer. The cross-linked PbS NC thin films were fabricated with a sequential layer-by-layer spin-casting method. Instead of widely used 1,4-benzenedithiol,[32] in this work, we used 1,3-benzenedithiol (BDT) as the cross-linker to replace oleic acid and bridge the NCs. Each NC layer was spin-cast at 5000 rpm for 1 min with a thickness of 6−7 nm, corresponding to 1−2 monolayers of the NC. After casting an NC layer, the substrate was soaked into a 0.02 M BDT in acetonitrile for 30s, then immediately removed from the solution and spun at 5000 rpm for 1 min to quickly dry the film. A desired film thickness was achieved by repeating this process. Afterward, the sample was transferred to an evaporation chamber without exposure to the air. Finally, 1 nm of LiF and 120 nm of Al were thermally evaporated on top of the NC layer to form the cathode. The PV cells had a general structure of ITO/PbS-BDT (100−120 nm)/LiF (1 nm)/Al (120 nm) with an active area of 9 mm^2. The film thicknesses were measured by a Dektak profilometer.

The photovoltaic characteristics were characterized under one sun of simulated Air Mass 1.5 Global (AM 1.5G) solar irradiation (100 mW cm^{-2}, Sciencetech, Inc., SF150) at room temperature in a nitrogen-purged glovebox. The light intensity was measured with a power meter (Gentec, Inc., UP19K-30H-H5). After the current−voltage (*J*−*V*) measurement, the samples were exposed in air for the external quantum efficiency (EQE) measurements. The device power conversion efficiencies (PCEs) were calibrated using the short-circuit current density (J_{SC}) derived from the EQE data.

RESULTS AND DISCUSSION

In order to eliminate the variation in PV performance caused by the quantum size effect of the nanocrystals, the PbS nanocrystals synthesized in this study had the first excitonic peak λ_{1ex} at ~1100 nm ± 100 nm. It corresponds to a nanocrystal size of 4.5 nm ± 0.5 nm. Our previous study also showed that, at this size, the PbS PV cells had the highest PCE, with <15% variation in device performance.[30] To control the growth rate of the nanocrystals, we first varied the molar ratio of OA to Pb from 2.5:1 to 25:1. For different OA to Pb ratios, the concentration of OA in ODE was kept at ~0.5 mol/kg. Figure 1a and 1b show the temporal evolution of the absorption spectra of the PbS nanocrystals synthesized with molar ratios of OA to Pb at 2.5:1 and 12:1, respectively. The position and width of the fist excitonic peak represent the size and size distribution of the nanocrystals, respectively. As shown in Figure 1a, with a OA:Pb molar ratio of 2.5:1 in the synthesis, nucleation takes place very rapidly, right after the injection of the S precursor, and the solution turns black within a few seconds. Although the PbS NCs obtained after 1 min of growth showed a nice size distribution, such character was lost quickly after another minute of growth, and no clear size-focused stage could be observed. Slowing down the size-focusing stage in the growth of PbS nanocrystals can be achieved by increasing the molar ratio of OA to PbS. As shown in Figure 1b, with a OA:Pb molar ratio of 12:1, the time required to obtain the size-focused PbS NCs extends to 3 min, and the growth has more than 30 min

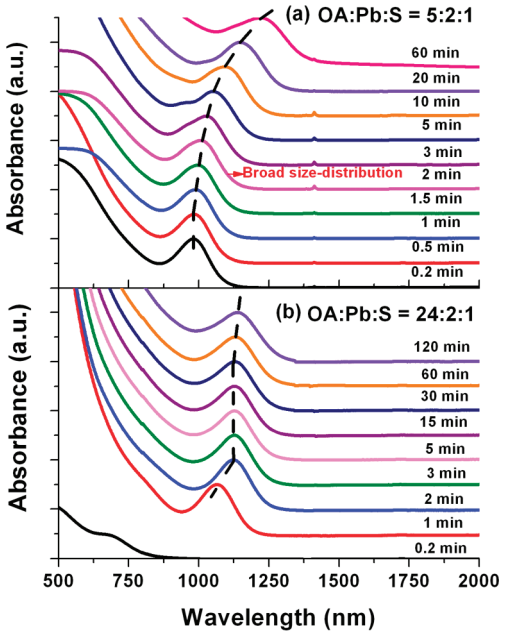

Figure 1. Temporal evolution of the absorption spectra of the PbS nanocrystals synthesized with an OA:Pb molar ratio of (a) 2.5:1 and (b) 12:1, respectively. The OA concentration in ODE was 0.44 and 0.51 mol/kg, respectively.

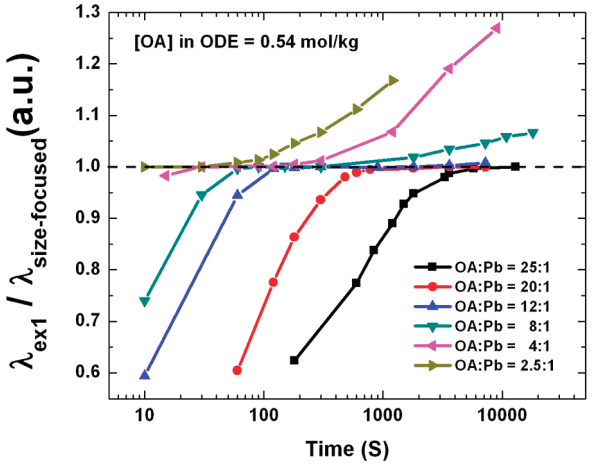

Figure 2. Temporal evolution of the normalized first excitonic peak $\lambda_{1ex}/\lambda_{size\text{-}focused}$ of the PbS nanocrystals with different feed molar ratios of OA to Pb. The concentration of OA in ODE in all the cases is kept at 0.54 mol/kg.

of "size-focused" stage before the Ostwald ripening process takes place. This stage is particularly important for the extraction of monodispersed and size-stable nanocrystals. In addition, the first excitonic peak of the obtained PbS nanocrystals showed a narrow full-width-at-half-maximum (fwhm) of 165 nm, indicating a narrow size distribution of the nanocrystals.[33] Figure 2 shows the temporal evolution of the first excitonic peak position of PbS NCs synthesized with different molar ratios (2.5:1 to 25:1) of OA to Pb. Clear and prolonged size-focused stage was observed when the molar ratio is higher than 8:1. The time to reach the size-focused stage in nanocrystal growth for different molar ratios is summarized in Table 1. Another approach to

Table 1. Summary of the Time Required to Obtain the Size-Focused PbS NCs with Similar Sizes at Different OA:Pb Feed Molar Ratios of and a Fixed OA Concentration (0.54 mol/kg)

OA:Pb molar ratio	time required to get the size-focused PbS NCs (min)
2.5:1	N/A
4:1	0.5
8:1	1.5
12:1	3
20:1	30
25:1	>60

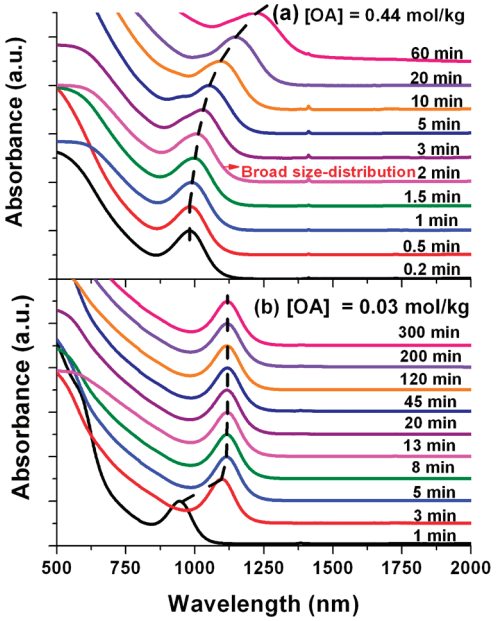

Figure 3. Temporal evolution of the absorption spectra of the PbS nanocrystals synthesized with a concentration of OA in ODE at (a) 0.44 mol/kg and (b) 0.03 mol/kg. The OA:Pb molar ratio in both cases was 2.5:1.

extend the size-focusing stage in PbS NC growth is to greatly dilute both the lead and sulfur precursors with ODE. Figure 3a and 3b show temporal evolution of the absorption spectra of the PbS nanocrystals synthesized with the same OA:Pb molar ratio of 2.5:1 but a factor of ~15 difference in reactant concentration. Diluting the concentration of the precursors not only reduced the reactivity of the nanocrystal growth, but also resulted in a narrow size distribution and prolonged size-focused stage. However, extremely low reactant concentration is not practical, because only a small amount of nanocrystals can be obtained after purification. It is worth pointing out that, at high OA/Pb ratio (8:1 was studied), high-quality PbS NCs can still be obtained, even with high OA concentration (1.51 mol/kg). Under this condition, PbS NCs can be synthesized at a large scale for practical applications.

Figures 4a and 4b show the typical TEM images of the fast and slow growth PbS NCs, respectively. Both NCs are almost monodispersed. The average distance between two adjacent nanocrystals is ~2.0 nm, which is similar to the length of the OA molecule, indicating that the nanocrystals are closely packed and passivated by the OA ligands. Moreover, as demonstrated in PV devices, monodispersity has no notable impact on device

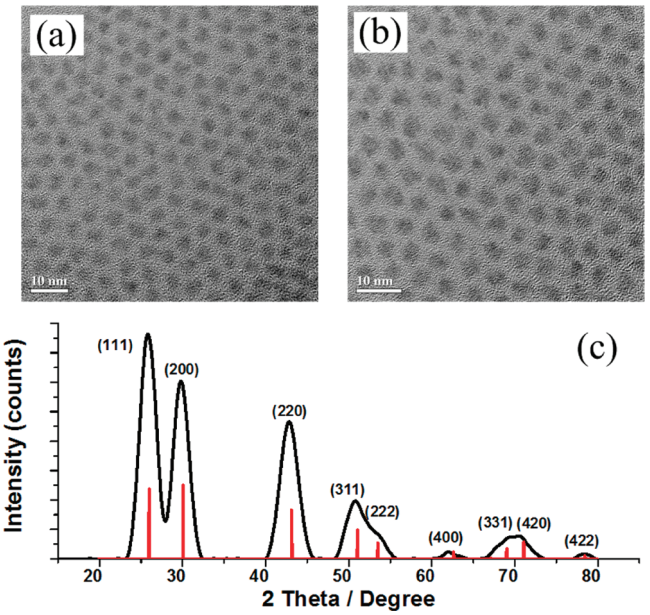

Figure 4. TEM images of as-synthesized (a) fast and (b) slow growth PbS nanocrystals. (c) Typical XRD pattern of PbS nanocrystals (black) and bulk PbS (red).

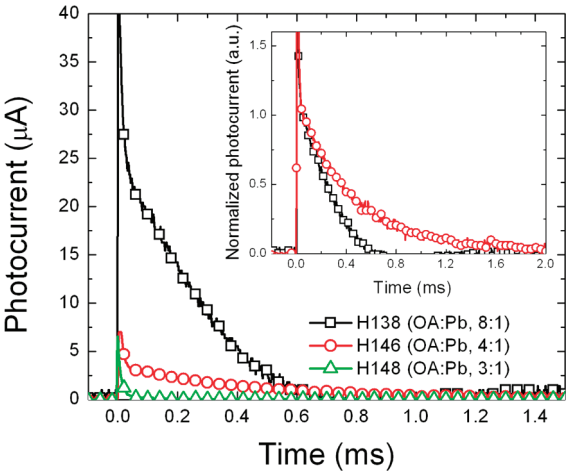

Figure 5. Transient photocurrent (TPC) signals of nanocrystal thin films which synthesized with different oleic acid to Pb (OA:Pb) molar ratios ((black square) 8:1, (red circle) 4:1, and (green triangle) 3:1). The films were excited with a pulsed nitrogen laser at $t = 0$ s.

performance (see the Supporting Information). Figure 4c shows a typical XRD pattern of the as-synthesized NCs; both fast and slow growth NCs also show similar crystallinity. High-resolution XPS results of the fast and slow growth NCs also showed similar results with a lead-rich NC surface, and a high number of carbon (C═O) to lead ratio (0.5) (see the Supporting Information). The C═O bond is originated from the oleic acid surface ligand. As discussed by Lobo et al.,[34] such a high number of C═O to lead ratio suggests that the oleic acid molecules outnumber the surface Pb atoms, and it indicates that the oleic acid ligands were bound preferentially to the Pb atoms on the nanocrystal surface. No significant difference was found between the slow and fast growth NCs, using the above spectroscopic techniques. One possible reason is the amount of possible defects in the NCs is too small to be resolved by the spectroscopic techniques. It is commonly found in conventional semiconductors that even a very low impurity level—a few orders of magnitude lower than the atomic density—can have significant impact on the device performance.

We further sought to compare the fast and slow growth NCs using transient photocurrent (TPC) technique. TPC takes into account the accumulative effect of the trapping and detrapping processes of charge carriers inside the materials. The acquired TPC signal is sensitive to any defect or trap states, and it has been widely used to study different electronic materials.[35−38] At zero external voltage bias, the photogenerated carriers near to the front electrode (ITO) must diffuse across the NC thin film to the back electrode (Al) to generate electric current. Consequently, a charge carrier (electron in this case) must go through successive trapping and detrapping processes in order to transport from one electrode to another. Therefore, a strong photocurrent and small decay time constant will indicate a low trap density and good charge transport properties. We fabricated cross-linked PbS NCs thin films with NCs synthesized with OA:Pb molar ratios of 3:1, 4:1, and 8:1. The thicknesses of the films were ∼200 nm, which were larger than the depletion width (80 nm) determined by capacitance−voltage ($C-V$) measurement, ensuring that diffusion was the major carrier transport mechanism across the film. The NCs prepared using different recipes were chosen to have their first excitonic peaks at 1100 nm ± 30 nm. Figure 5 shows the TPC signals of different samples after excitation of a pulsed nitrogen laser at $t = 0$ s. At first glance, the film of slow-growth NCs has a larger photocurrent signal. The photocurrent decay is faster in films fabricated using slower-growth NCs. The magnitude and decay time constant of the photocurrent are very sensitive to the trap states in the NC thin film. In the films of fast-growth NCs synthesized with a OA:Pb molar ratio of 3:1, the photocurrent is too weak to be used for extracting its decay time constant. This result provides a strong evidence of reduced trap density in the resulting NC thin film made from slow-growth NCs. The result is consistent with the larger short-circuit current and smaller series resistance obtained in PV devices with slow-growth NCs.

From the TPC results, we have found that the slow-growth synthesis leads to reduced trap density in the NCs. With no doubt, the presence of trap states has direct impact on the electronic device performance. In order to investigate such correlation, we fabricated a series of photovoltaic devices with PbS nanocrystals synthesized with different growth rates. For each synthesis, the nanocrystals were extracted at the onset of the size-focused stage. It should be noted that when the nanocrystal growth was stopped before the size-focusing stage, the resulting PV devices showed a low PCE of ∼1.8%.

Shottky-type PV cells were fabricated and the details of the processes are discussed in the Experimental Section. Over 30 batches of NCs with similar sizes were evaluated. The first excitonic peaks of these NCs are ∼1100 nm ± 100 nm. For each batch of the NCs, the devices were optimized by the NC layer thickness. Figure 6 shows the photovoltaic device performance with nanocrystals synthesized with different size-focusing time, the time required to obtain the size-focused nanocrystals. Each data point represents at least 3 batches of nanocrystals and over 20 devices. The devices fabricated with the fast-growth nanocrystals have an overall PCE of 2.0%, which is comparable to the literature values for PbS NCs synthesized under similar condition.[16] While the PbS NCs synthesized with the slow-growth recipes show remarkable photovoltaic performance, with PCEs over 3.0% in

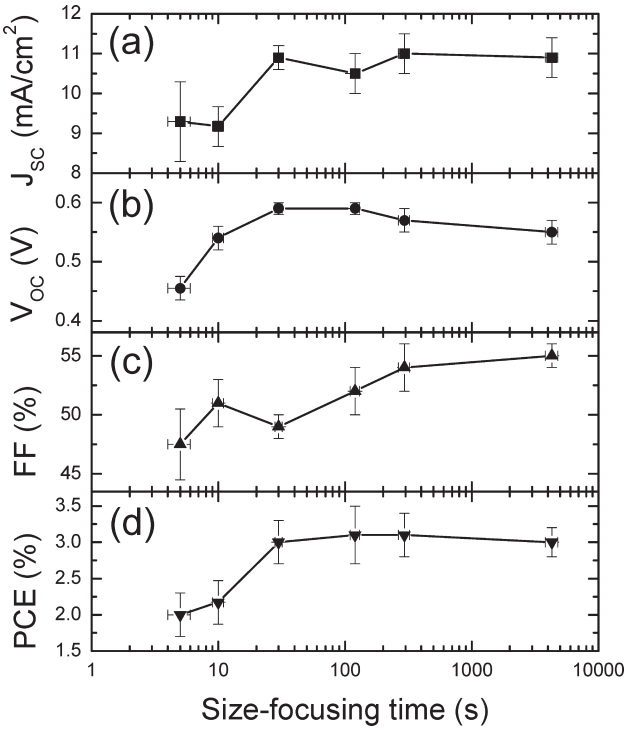

Figure 6. PbS nanocrystals photovoltaic performance ((a) J_{SC}, (b) V_{OC}, (c) *FF*, and (d) PCE) versus the size-focusing time of the nanocrystals needed during the synthesis. The size-focusing time represents the time required to reach the size-focused stage during the growth of nanocrystals. The error bar represents the standard derivation of an ensemble of samples.

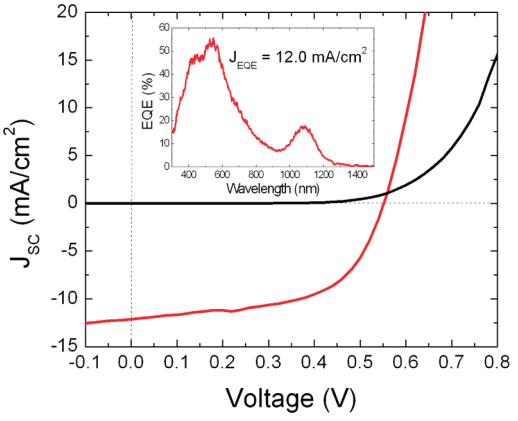

Figure 7. Measured current density−voltage ($J - V$) characteristics under one sun of simulated AM 1.5G solar irradiation of a Schottky-type PbS NCs PV cell with the nanocrystal synthesized by slow-growth process. The external quantum efficiency (EQE) of the device is shown in the inset. An integrated current of 12.0 mA/cm^2 is obtained from the EQE data, with respect to AM 1.5G illumination.

more than 20 batches of nanocrystals tested. The high device efficiency is mostly due to the improvement in V_{OC} and *FF*. The V_{OC} increased from 0.45 V to 0.55 V and was close to the upper limit imposed by the half-energy bandgap of the nanocrystals (1.1−1.2 eV). The *FF* also increased from 47% to 55%. Figure 7 shows the current density−voltage (J−V) characteristics and the external quantum efficiency (EQE) of our best PbS PV device

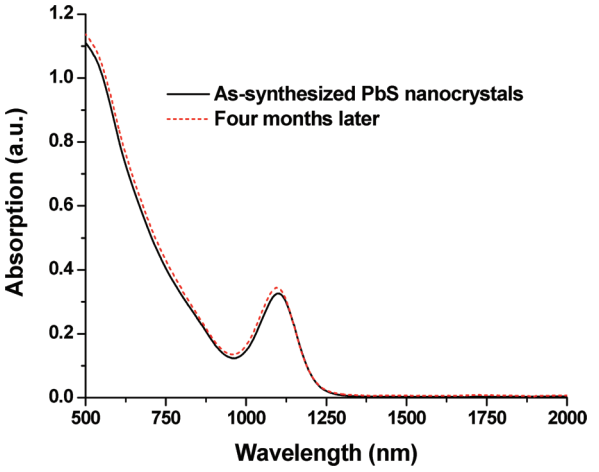

Figure 8. Absorption spectra of PbS nanocrystals in TCE measured as-synthesized and after being stored at −20 °C with no protection of any inert gases for four months.

with nanocrystals synthesized with the slow-growth process, with a PCE of 3.8% under AM 1.5G irradiation at 100 mW/cm^2. Such efficiency is the highest among those nanocrystal PV cells reported in the literature. A short-circuit current (J_{SC}) of 12.1 mA/cm^2 obtained from the I−V measurement is consistent with the calculated J_{SC} (12.0 mA/cm^2) from the EQE data. The open-circuit voltage (V_{OC}) of 0.54 V is approximately half of the energy bandgap of the PbS NC. The impeccable V_{oc} and a high fill-factor (*FF*) of 59% suggest low recombination loss and trap state density in the device, which is a direct proof of the improved nanocrystal quality when using the slow-growth process. Furthermore, the slow-growth NCs also show long-term stability. As shown in Figure 8, there is negligible change in the absorption spectra, even after four months of storage in a freezer (−20 °C) without any inert gases protection. The stability of the nanocrystals is also confirmed by the PV device performance. The devices fabricated from the PbS NCs with different storage time have consistent power conversion efficiencies (see Table S1 in the Supporting Information).

CONCLUSIONS

In summary, we have demonstrated the control of the growth rate of PbS nanocrystals by controlling the feed molar ratio of OA to Pb and the precursor concentration in ODE. A prolonged size-focused stage is obtained with the slow-growth recipes, which facilitates the extraction of monodispersed and stable nanocrystals from the reaction. More importantly, we found that the slow-growth nanocrystals have reduced trap density. Photovoltaic devices fabricated with the slow-growth nanocrystal have a 2-fold increase in power conversion efficiency (PCE). It is attributed to the remarkable improvement in the open-circuit voltage and fill factor. A state-of-the-art PCE of 3.8% is obtained in PbS nanocrystal PV devices using the slow-growth nanocrystals.

ASSOCIATED CONTENT

Supporting Information. XPS spectra, TEM images, PL spectra, FTIR spectra, summaries of the photovoltaic performance for the PbS nanocrystals with different storage time, nanocrystal monodispersivity on PV device performance, and PbS nanocrystal

dx.doi.org/10.1021/cm200051j |*Chem. Mater.* 2011, 23, 1805–1810

PV device performance at different light intensities. This material is available free of charge via the Internet at http://pubs.acs.org.

AUTHOR INFORMATION

Corresponding Author

*E-mails: jianping.lu@nrc-cnrc.gc.ca (J.L.); kui.yu@nrc-cnrc.gc.ca (K.Y.); ye.tao@nrc-cnrc.gc.ca (Y.T.).

ACKNOWLEDGMENT

This work was supported by NRC-Nano Initiative at the National Research Council of Canada (NRC). The authors thank Dashan Wang for the HRTEM imaging, Xiaohua Wu for the TEM imaging, David Kingston and Zhenhua He for the XPS characterization, and Zhiyuan Wang and Peter Mirtchev at Carleton University for NIR photoluminescence measurements, as well as Yi Tang and Qingsheng Gao at Fudan University and Md. Badruz Zaman, Ruibing Wang, and Salem Wakim at NRC for the helpful discussions. H.F. thanks the Chinese Scholarship Council for providing her PDF scholarship.

REFERENCES

(1) Alivisatos, A. P. *Science* **1996**, *271*, 933–937.
(2) Nirmal, M.; Brus, L. *Acc. Chem. Res.* **1999**, *32*, 407–414.
(3) Colvin, V. L.; Schlamp, M. C.; Alivisatos, A. P. *Nature* **1994**, *370*, 354–357.
(4) Huynh, W. U.; Dittmer, J. J.; Alivisatos, A. P. *Science* **2002**, *295*, 2425–2427.
(5) Krasteva, N.; Besnard, I.; Guse, B.; Bauer, R. E.; Mullen, K.; Yasuda, A.; Vossmeyer, T. *Nano Lett.* **2002**, *2*, 551–555.
(6) Bruchez, M.; Moronne, M.; Gin, P.; Weiss, S.; Alivisatos, A. P. *Science* **1998**, *281*, 2013–2016.
(7) Jain, P. K.; Huang, X. H.; El-Sayed, I. H.; El-Sayed, M. A. *Acc. Chem. Res.* **2008**, *41*, 1578–1586.
(8) Sun, S. H.; Murray, C. B.; Weller, D.; Folks, L.; Moser, A. *Science* **2000**, *287*, 1989–1992.
(9) Kasuya, A.; Sivamohan, R.; Barnakov, Y. A.; Dmitruk, I. M.; Nirasawa, T.; Romanyuk, V. R.; Kumar, V.; Mamykin, S. V.; Tohji, K.; Jeyadevan, B.; Shinoda, K.; Kudo, T.; Terasaki, O.; Liu, Z.; Belosludov, R. V.; Sundararajan, V.; Kawazoe, Y. *Nat. Mater.* **2004**, *3*, 99–102.
(10) Sun, L. F.; Bao, L.; Hyun, B. R.; Bartnik, A. C.; Zhong, Y. W.; Reed, J. C.; Pang, D. W.; Abruna, H. D.; Malliaras, G. G.; Wise, F. W. *Nano Lett.* **2009**, *9*, 789–793.
(11) Wise, F. W. *Acc. Chem. Soc.* **2000**, *33*, 773–780.
(12) Murphy, J. E.; Beard, M. C.; Norman, A. G.; Ahrenkiel, S. P.; Johnson, J. C.; Yu, P. R.; Mićić, O. I.; Ellingson, R. J.; Nozik, A. J. *J. Am. Chem. Soc.* **2006**, *128*, 3241–3247.
(13) Johnston, K. W.; Pattantyus-Abraham, A. G.; Clifford, J. P.; Myrskog, S. H.; MacNeil, D. D.; Levina, L.; Sargent, E. H. *Appl. Phys. Lett.* **2008**, *92*, 151115.
(14) Sargent., E. H. *Nat. Photonics* **2009**, *3*, 325–331.
(15) Luther, J. M.; Law, M.; Beard, M. C.; Song, Q.; Reese, M. O.; Ellingson, R. J.; Nozik, A. J. *Nano Lett.* **2008**, *8*, 3488–3492.
(16) Ma, W. L.; Luther, J. M.; Zheng, H. M.; Wu, Y.; Alivisatos, A. P. *Nano Lett.* **2009**, *9*, 1699–1703.
(17) Choi, J. J.; Lim, Y. F.; Santiago-Berrios, M. B.; Oh, M.; Hyun, B. R.; Sun, L. F.; Bartnik, A. C.; Goedhart, A.; Malliaras, G. G.; Abruna, H. D.; Wise, F. W.; Hanrath, T. *Nano Lett.* **2009**, *9*, 3749–3755.
(18) Konstantatos, G.; Howard, I.; Fischer, A.; Hoogland, S.; Clifford, J.; Klem, E.; Levina, L.; Sargent, E. H. *Nature* **2006**, *442*, 180–183.
(19) Schaller, R. D.; Petruska, M. A.; Klimov, V. I. *J. Phys. Chem. B* **2003**, *10*, 13765–13768.
(20) Steckel, J. S.; Coe-Sullivan, S.; Bulović, V.; Bawendi, M. G. *Adv. Mater.* **2003**, *15*, 1862–1866.
(21) Yang, R. Y.; Feser, J. P.; Lee, J. S.; Talapin, D. V.; Segalman, R.; Majumdar, A. *Nano Lett.* **2008**, *8*, 2283–2288.
(22) Hines, M. A.; Scholes, G. D. *Adv. Mater.* **2003**, *15*, 1844–1849.
(23) Abel, K. A.; Shan, J. N.; Boyer, J.-C.; Harris, F.; van Veggel, F. C. J. M. *Chem. Mater.* **2008**, *20*, 3794–3796.
(24) Tsang, S. W.; Fu, H.; Wang, R.; Lu, J.; Yu, K.; Tao, Y. *Appl. Phys. Lett.* **2009**, *95*, 183505.
(25) Debnath, R.; Tang, J.; Barkhouse, D. A.; Wang, X.; Pattantyus-Abraham, A. G.; Brzozowski, L.; Levina, L.; Sargent, E. H. *J. Am. Chem. Soc.* **2010**, *132*, 5952–5953.
(26) Leschkies, K. S.; Beatty, T. J.; Kang, M. S.; Norris, D. J.; Aydil, E. S. *ACS Nano* **2009**, *3*, 3638–3648.
(27) Choi, J. J.; Lim, Y.-F.; Santiago-Berrios, M. B.; Oh, M.; Hyun, B.-R.; Sun, L.; Bartnik, A. C.; Goedhart, A.; Malliaras, G. G.; Abruña, H. D.; Wise, F. W.; Hanrath, T. *Nano Lett.* **2009**, *9*, 3749–3755.
(28) Luther, J. M.; Gao, J.; Lloyd, M. T.; Semonin, O. E.; Beard, M. C.; Nozik, A. J. *Adv. Mater.* **2010**, *22*, 3704–3707.
(29) Pattantyus-Abraham, A. G.; Kramer, I. J.; Barkhouse, A. R.; Wang, X.; Konstantatos, G.; Debnath, R.; Levina, L.; Raabe, I.; Nazeeruddin, M. K.; Grätzel, M.; Sargent, E. H. *ACS Nano* **2010**, *4*, 3374–3380.
(30) Tsang, S. W.; Fu, H.; Ouyang, J.; Zhang, Y.; Yu, K.; Lu, J.; Tao, Y. *Appl. Phys. Lett.* **2010**, *96*, 243104.
(31) Yu, W. W.; Peng, X. G. *Angew. Chem., Int. Ed.* **2002**, *41*, 2368–2371.
(32) Koleilat, G. I.; Levina, L.; Harnik, S.; Myrskog, S. H.; Hinds, S.; Pattantyus-Abraham, A. G.; Sargent, E. H. *ACS Nano* **2008**, *2*, 833–840.
(33) Pesika, N. S.; Stebe, K. J.; Searson, P. C. *Adv. Mater.* **2003**, *15*, 1289–1291.
(34) Lobo, A.; Möller, T.; Nagel, M.; Borchert, H.; Hickey, S. G.; Weller, H. *J. Phys. Chem. B* **2005**, *109*, 17422–17428.
(35) Orenstein, J.; Kastner, M. *Phys. Rev. Lett.* **1981**, *46*, 1421.
(36) Tiedje., T.; Cebulka, J. M.; Morel, D. L.; Abeles, B. *Phys. Rev. Lett.* **1981**, *46*, 1425.
(37) Walker, A. B.; Peter, L. M.; Martinez, D.; Lobato, K. *Chimia* **2007**, *61*, 792–795.
(38) McNeill, C. R.; Hwang, I.; Greenham, N. C. *J. Appl. Phys.* **2009**, *106*, 024507.